Numerical Heat Transfer, Part A, 41: 65–87, 2002

1040-7782/02 $12.00+ .00

DOUBLE-DIFFUSIVE CONVECTION IN A POROUS ENCLOSURE WITH COOPERATING TEMPERATURE AND CONCENTRATION GRADIENTS AND HEAT GENERATION OR ABSORPTION EFFECTS

Ali J. Chamkha
Department of Mechanical Engineering, Kuwait University, Safat, Kuwait

The problem of unsteady, laminar double-diffusive convective flow of a binary gas mixture in a rectangular enclosure filled with a uniform porous medium is considered. A temperature-dependent heat source or sink is assumed to exist within the enclosure boundaries. Transverse cooperating gradients of heat and mass are applied on the two opposing vertical walls of the enclosure while the other two horizontal walls are adiabatic and impermeable to mass transfer. A numerical solution based on the finite-difference methodology is obtained. Representative results illustrating the effects of the inverse Darcy number, the heat generation or absorption coefficient, and the buoyancy ratio on the contour maps of the streamline, temperature, and concentration as well as the profiles of velocity, temperature, and concentration at the midsection of the enclosure are reported. In addition, results for the average Nusselt and Sherwood numbers are presented in tabulated form and discussed for various parametric conditions.

INTRODUCTION

Double-diffusive convection refers to buoyancy-driven flows induced by combined temperature and concentration gradients. The cases of cooperating thermal and concentration buoyancy forces where both forces act in the same direction and opposing thermal and concentration buoyancy forces where both forces act in opposite directions have been considered in the literature. Double diffusion occurs in a wide range of scientific fields such as oceanography, astrophysics, geology, biology, and chemical processes (see, for instance, Beghein et al. [1]). Ostrach [2] and Viskanta et al. [3] have reported complete reviews on the subject. Lee and Hyun [4] and Hyun and Lee [5] have reported numerical solutions for double-diffusive convection in a rectangular enclosure with aiding and opposing temperature and concentration gradients. Their solutions were compared favorably with reported experimental results. Mamou et al. [6] have reported an analytical and numerical study of double-diffusive convection in a vertical enclosure. The phenomenon of deep interface

Received 26 January 2001; accepted 6 July 2001.
Address correspondence to Professor A. J. Chamkha, Department of Mechanical & Industrial Engineering, Kuwait University, P. O. Box 5969, Safat, 13060 Kuwait.
E-mail: chamkha@kuc01.kuniv.edu.kw

NOMENCLATURE

A	enclosure aspect ratio = H/W	v	vertical velocity component
c	concentration of species	V	dimensionless vertical velocity component = vW/α_e
C	dimensionless species concentration = $(c - c_1)/(c_h - c_l) - 0.5$	W	enclosure width
c_h	high species concentration (source)	x	horizontal coordinate
c_l	low species concentration (sink)	X	dimensionless horizontal coordinate = x/W
D	species diffusivity	y	vertical coordinate
Da*	Darcy number = W^2/κ	Y	dimensionless vertical coordinate = y/W
g	gravitational acceleration	α_e	effective thermal diffusivity of the porous medium
H	enclosure height	β_T	thermal expansion coefficient
Le	Lewis number = α_e/D	β_c	compositional expansion coefficient
N	buoyancy ratio = $\beta_c(c_h - c_l)/[\beta_T(T_h - T_c)]$	ϕ	dimensionless heat generation or absorption coefficient = $Q_0W^2/(\rho c_p\alpha_e)$
$\overline{\mathrm{Nu}}$	average Nusselt number at heated vertical wall	κ	permeability of the porous medium
P	fluid pressure	μ	dynamic viscosity
Pr	Prandtl number = ν/α_e	ν	kinematic viscosity = μ/ρ
Q_0	heat generation or absorption coefficient	θ	dimensionless temperature = $(T - T_c)/(T_h - T_c) - 0.5$
Ra	thermal Rayleigh number = $g\beta_T(T_h - T_c)W^3/(\alpha_e\nu)$	ρ	density
Sh	average Sherwood number at heated vertical wall	τ	dimensionless time = $\alpha_e t/W^2$
t	time	τ_0	period of oscillation
T	temperature	Ω	vorticity
T_c	cold wall temperature (sink)	ψ	dimensionless stream function = Ψ/α_e
T_h	hot wall temperature (source)	Ψ	stream function
u	horizontal velocity component	ζ	dimensionless vorticity = $\Omega W^2/\alpha_e$
U	dimensionless horizontal velocity component = uW/α_e	∇^2	Laplacian operator

depression or pit formation as a result of solute accumulation due to double-diffusive convection in the directional solidification of succinonitrile (SCN) containing ethanol in an ampoule has been investigated by Lan and Tu [7]. Mergui and Gobin [8] have studied transient double-diffusive convection in a vertical enclosure with asymmetrical boundary conditions. The three-dimensional aspects of thermosolutal natural convection in a cubic enclosure subject to horizontal and opposing gradients of heat and solute have been reported by Sezai and Mohamad [9]. Double-diffusive convection in an annular enclosure with a hot inner cylinder has been investigated by Wang et al. [10].

Recently, interest in studying double-diffusive convective flows induced by the combined action of both temperature and concentration gradients in porous media has surged in view of its importance in many engineering problems, such as migration of moisture contained in fibrous insulation, grain storage, the transport of contaminants in saturated soil, the underground disposal of nuclear wastes, and drying processes (Mamou et al. [11]). Trevisan and Bejan [12] have studied heat and mass transfer by natural convection in a vertical slot filled with a porous medium. Chen and Chen [13] have considered double-diffusive fingering convection in a porous medium. Lin [14] has studied unsteady natural convection heat and mass

transfer in a saturated porous medium. Mamou et al. [15] have analyzed double-diffusion convection in an inclined slot filled with a porous medium. Double-diffusive convection in an annular vertical porous layer has been studied by Marcoux et al. [16]. Shivakumara and Sumithra [17] have considered non-Darcian effects on double-diffusive convection in a sparsely packed porous medium. Mahidjiba et al. [18] have reported on the onset of double-diffusive convection in a rectangular porous cavity subject to mixed boundary conditions.

Natural convection heat transfer induced by internal heat generation has recently received considerable attention because of numerous applications in geophysics and energy-related engineering problems. Such applications include heat removal from nuclear fuel debris, underground disposal of radioactive waste materials, storage of foodstuff, and exothermic chemical reactions in packed-bed reactor (see, for instance, Kakac et al. [19]). Acharya and Goldstein [20] studied numerically two-dimensional natural convection of air in an externally heated vertical or inclined square box containing uniformly distributed internal energy sources. Their numerical results showed two distinct flow pattern systems depending on the ratio of the internal to the external Rayleigh numbers. Also, it was found that the average heat flux ratio along the cold wall increased with increasing external Rayleigh numbers and decreasing internal Rayleigh numbers. Recently, Churbanov et al. [21] studied numerically unsteady natural convection of a heat generating fluid in a vertical rectangular enclosure with isothermal or adiabatic rigid walls. Their results were obtained using a finite-difference scheme in the two-dimensional stream function vorticity formulation. Steady-state as well as oscillating solutions were obtained and compared with other numerical and experimental published data. Other related works dealing with temperature-dependent heat generation effects can be found in the papers by Vajravelu and Nayfeh [22] and Chamkha [23].

The objective of this work is to consider unsteady, laminar, double-diffusive natural convection flow inside a rectangular enclosure filled with a uniform porous medium with cooperating temperature and concentration gradients. This problem represents the opposite case of the works of Nishimura et al. [24] and Mamou et al. [11], who considered opposing temperature and concentration gradients. In addition, the present problem allows for the presence of heat generation or absorption effects. This type of flow and heat transfer situation finds application in many engineering and technological areas such as geothermal reservoirs, petroleum extraction, chemical catalytic reactors, prevention of subsoil water pollution, nuclear reactors, underground diffusion of nuclear wastes and other contaminants, and porous material regenerative heat exchangers.

MATHEMATICAL MODEL

Consider unsteady, laminar, two-dimensional double-diffusive convective flow inside a rectangular porous enclosure in the presence of internal heat generation or absorption effects. The temperatures T_h and T_c and concentrations c_h and c_l are uniformly imposed on the two opposing vertical walls such that $T_h > T_c$ and $c_h > c_l$ while the two horizontal walls are assumed to be adiabatic and impermeable to mass transfer. The left wall at T_h and c_h is the source where the mixture diffuses to the

opposing wall (sink). Figure 1 shows the schematic of the problem under consideration. The fluid is assumed to be incompressible, Newtonian, and viscous. The porous medium is assumed to be uniform and in local thermal and compositional equilibrium with the fluid. The effects due to viscous dissipation and porous medium inertia are assumed to be negligible.

The governing equations for this problem are based on the balance laws of mass, linear momentum, thermal energy, and concentration. Taking into account the assumptions mentioned above, and applying the Boussinesq approximation for the body force terms in the momentum equations, the governing equations can be written in dimensional form as

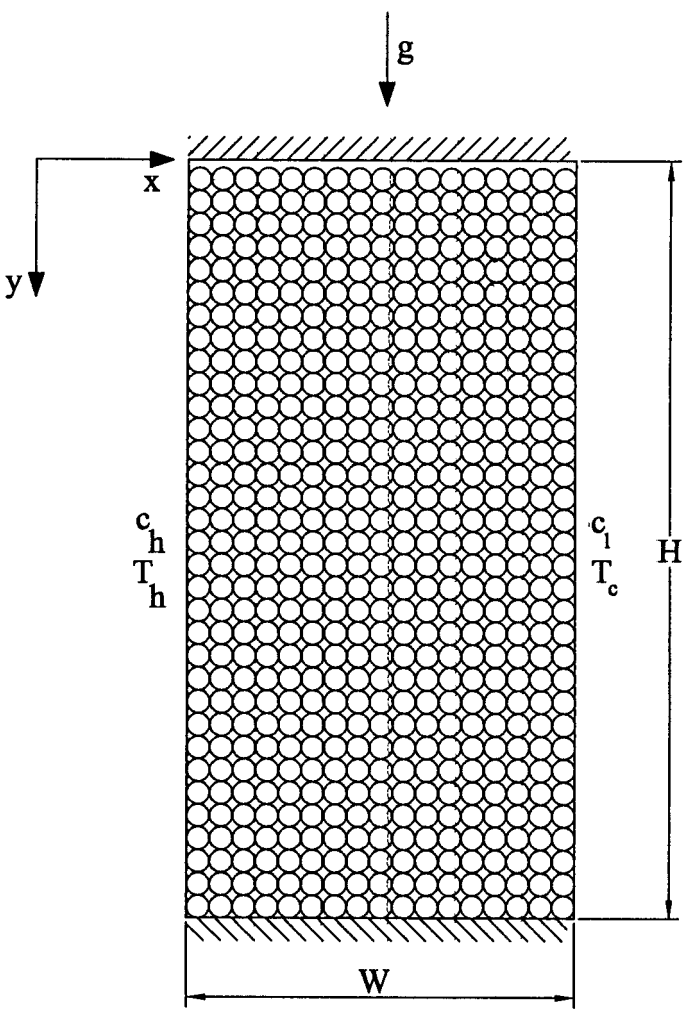

Figure 1. Schematic diagram of the porous enclosure.

$$\frac{\partial u}{\partial x}+\frac{\partial v}{\partial y}=0 \tag{1}$$

$$\frac{\partial u}{\partial t}+u\frac{\partial u}{\partial x}+v\frac{\partial u}{\partial y}=-\frac{1}{\rho}\frac{\partial p}{\partial x}+\nu\left(\frac{\partial^2 u}{\partial x^2}+\frac{\partial^2 u}{\partial y^2}\right)-\frac{\mu}{\rho\kappa}u \tag{2}$$

$$\frac{\partial v}{\partial t}+u\frac{\partial v}{\partial x}+v\frac{\partial v}{\partial y}=-\frac{1}{\rho}\frac{\partial p}{\partial y}+\nu\left(\frac{\partial^2 v}{\partial x^2}+\frac{\partial^2 v}{\partial y^2}\right)+g\beta_T(T-T_c)+g\beta_c(c-c_1)-\frac{\mu}{\rho\kappa}v \tag{3}$$

$$\frac{\partial T}{\partial t}+u\frac{\partial T}{\partial x}+v\frac{\partial T}{\partial y}=\alpha_e\left(\frac{\partial^2 T}{\partial x^2}+\frac{\partial^2 T}{\partial y^2}\right)+\frac{Q_0}{\rho c_p}(T-T_c) \tag{4}$$

$$\frac{\partial c}{\partial t}+u\frac{\partial c}{\partial x}+v\frac{\partial c}{\partial y}=D\left(\frac{\partial^2 c}{\partial x^2}+\frac{\partial^2 c}{\partial y^2}\right) \tag{5}$$

where x, y, and t are the horizontal and vertical distances and time, respectively. u, v, p, T, and c are the velocity components in the x- and y-directions, pressure, temperature, and concentration, respectively. β_T and β_c are the thermal and compositional expansion coefficients, respectively. The parameters κ, α_e, ν, μ c_p, and ρ are the permeability and effective thermal diffusivity of the porous medium, the fluid kinematic and dynamic viscosities, specific heat at constant pressure, and the fluid density, respectively. Q_0 is the heat generation ($Q_0>0$) or absorption ($Q_0<0$) coefficient, D is the species diffusivity, T_h and T_c are the hot and cold wall temperature, c_h and c_l are the concentration at the hot and cold walls, and g is the gravitational acceleration.

The boundary conditions for the problem can be written as

$$\begin{array}{llllll}
x=0 & y=y & u=0 & v=0 & T=T_h & c=c_h \\
x=W & y=y & u=0 & v=0 & T=T_c & c=c_l \\
x=x & y=0 & u=0 & v=0 & \dfrac{\partial T}{\partial y}=0 & \dfrac{\partial c}{\partial y}=0 \\
x=x & y=H & u=0 & v=0 & \dfrac{\partial T}{\partial y}=0 & \dfrac{\partial c}{\partial y}=0
\end{array} \tag{6}$$

where W and H are the width and height of the enclosure, respectively.

The dimensional stream function and vorticity can be defined in the usual way as

$$u=\frac{\partial \Psi}{\partial y} \quad v=-\frac{\partial \Psi}{\partial x} \quad \Omega=-\left(\frac{\partial^2 \Psi}{\partial x^2}+\frac{\partial^2 \Psi}{\partial y^2}\right) \tag{7}$$

It is convenient to nondimensionalize Eqs. (1) through (7) by using the following dimensionless variables:

$$X = \frac{x}{W} \quad Y = \frac{y}{W} \quad \tau = \frac{\alpha_e t}{W^2} \quad \zeta = \frac{\Omega W^2}{\alpha_e} \quad \psi = \frac{\Psi}{\alpha_e} \quad \theta = \frac{(T - T_c)}{(T_h - T_c)} - 0.5$$
$$C = \frac{(c - c_l)}{(c_h - c_l)} - 0.5 \quad \mathrm{Pr} = \nu/\alpha_e \quad \mathrm{Da}^* = \frac{W^2}{\kappa} \quad N = \frac{\beta_c(c_h - c_l)}{\beta_T(T_h - T_c)}$$
$$\mathrm{Le} = \frac{\alpha_e}{D} \quad \mathrm{Ra} = \frac{g\beta_T(T_h - T_c)W^3}{\alpha_e \nu} \quad \phi = \frac{Q_0 W^2}{\rho c_p \alpha_e} \tag{8}$$

where the dimensionless parameters appearing in the above equations are given in the nomenclature list.

By employing Eqs. (8) and combining Eqs. (2) and (3) by eliminating the pressure gradient terms, the resulting dimensionless equations can be written as

$$\zeta = \frac{\partial V}{\partial X} - \frac{\partial U}{\partial Y} = -\nabla^2 \psi \tag{9}$$

$$\frac{\partial \zeta}{\partial \tau} + U\frac{\partial \zeta}{\partial X} + V\frac{\partial \zeta}{\partial Y} = \mathrm{Pr}\nabla^2 \zeta + \mathrm{Ra}\ \mathrm{Pr}\left(\frac{\partial \theta}{\partial X} + N\frac{\partial C}{\partial X}\right) - \mathrm{Da}^*\mathrm{Pr}\,\zeta \tag{10}$$

$$\frac{\partial \theta}{\partial \tau} + U\frac{\partial \theta}{\partial X} + V\frac{\partial \theta}{\partial Y} = \nabla^2 \theta + \phi(\theta + 0.5) \tag{11}$$

$$\frac{\partial C}{\partial \tau} + U\frac{\partial C}{\partial X} + V\frac{\partial C}{\partial Y} = \nabla^2 C/\mathrm{Le} \tag{12}$$

The boundary conditions in dimensionless form become

$Y = 0$:

$$U = V = \psi = 0 \quad \zeta = -\left(\frac{\partial^2 \psi}{\partial Y^2}\right) \quad \frac{\partial \theta}{\partial Y} = 0 \quad \frac{\partial C}{\partial Y} = 0 \tag{13a}$$

$Y = H/W$:

$$U = V = \psi = 0 \quad \zeta = -\left(\frac{\partial^2 \psi}{\partial Y^2}\right) \quad \frac{\partial \theta}{\partial Y} = 0 \quad \frac{\partial C}{\partial Y} = 0 \tag{13b}$$

$X = 0$:

$$U = V = \psi = 0 \quad \zeta = -\left(\frac{\partial^2 \psi}{\partial X^2}\right) \quad \theta = 0.5 \quad C = 0.5 \tag{13c}$$

$X = 1$:

$$U = V = \psi = 0 \quad \zeta = -\left(\frac{\partial^2 \psi}{\partial X^2}\right) \quad \theta = -0.5 \quad C = -0.5 \tag{13d}$$

The average Nusselt and Sherwood numbers at the left heated vertical wall of the enclosure are given by

$$\overline{\mathrm{Nu}} = -\int_0^A \left(\frac{\partial \theta}{\partial X}\right) dY \tag{14}$$

$$\overline{\mathrm{Sh}} = -\int_0^A \left(\frac{\partial C}{\partial X}\right) dY \tag{15}$$

where $A = H/W$ is the enclosure aspect ratio.

NUMERICAL ALGORITHM

The numerical algorithm used to solve Eqs. (9) through (13) is based on the finite-difference methodology. Central difference quotients were used to approximate the second derivatives in both the X and Y directions. The governing equations are then transformed into tridiagonal algebraic equations, which were solved in the X- and Y-directions for the concentration, temperature, vorticity, and the stream function. This method was found to be stable and gave results that are very close to the numerical results obtained by Nishimura et al. [24] using the finite-element method.

As an example, the finite-difference formulation for Eq. (10) will have the form

$$\begin{aligned}
&\frac{[\zeta_{i,j}^{n+1} - \zeta_{i,j}^{n}]}{\Delta\tau} + U_{i,j}\frac{[\zeta_{i+1,j}^{n+1} - \zeta_{i-1,j}^{n+1}]}{2\Delta X} + V_{i,j}\frac{[\zeta_{i,j+1}^{n} - \zeta_{i,j-1}^{n}]}{2\Delta Y} \\
&\quad = \mathrm{Pr}\left\{\frac{[\zeta_{i+1,j}^{n+1} - 2\zeta_{i,j}^{n+1} + \zeta_{i-1,j}^{n+1}]}{\Delta X^2} + \frac{[\zeta_{i,j+1}^{n} - 2\zeta_{i,j}^{n+1} + \zeta_{i,j-1}^{n}]}{\Delta Y^2}\right\} \\
&\qquad + \mathrm{Ra}\,\mathrm{Pr}\left\{\frac{[\theta_{i+1,j} - \theta_{i-1,j}]}{2\Delta X} + N\frac{[C_{i+1,j} - C_{i-1,j}]}{2\Delta X}\right\} - \mathrm{Da}^{*}\mathrm{Pr}\,\zeta_{i,j}^{n+1}
\end{aligned} \tag{16a}$$

which can be rearranged as

$$\zeta_{i-1,j}^{n+1}[E_1] + \zeta_{i,j}^{n+1}[B_1] + \zeta_{i+1,j}^{n+1}[A_1] = [D_1] \tag{16b}$$

where

$$E_1 = \left[-\frac{U_{i,j}\Delta\tau}{2\Delta X} - \frac{\mathrm{Pr}\,\Delta\tau}{\Delta X^2}\right] \qquad B_1 = \left[1.0 + \frac{2\,\mathrm{Pr}\,\Delta\tau}{\Delta X^2} + \frac{2\,\mathrm{Pr}\,\Delta\tau}{\Delta Y^2} + \Delta\tau\mathrm{Da}^{*}\mathrm{Pr}\right]$$

$$A_1 = \left[\frac{U_{i,j}\Delta\tau}{2\Delta X} - \frac{\mathrm{Pr}\Delta\tau}{\Delta X^2}\right]$$

$$\begin{aligned}
D_1 = {} & \zeta_{i,j+1}^{n}\left[-\frac{V_{i,j}\Delta\tau}{2\Delta Y} + \frac{\mathrm{Pr}\,\Delta\tau}{\Delta Y^2}\right] + \zeta_{i,j}^{n}[1.0] + \zeta_{i,j-1}^{n}\left[\frac{V_{i,j}\Delta\tau}{2\Delta Y} + \frac{\mathrm{Pr}\,\Delta\tau}{\Delta Y^2}\right] \\
& + \mathrm{Ra}\,\mathrm{Pr}\Delta\tau\left\{\frac{[\theta_{i+1,j} - \theta_{i-1,j}]}{2\Delta X} + N\frac{[C_{i+1,j} - C_{i-1,j}]}{2\Delta X}\right\}
\end{aligned} \tag{16c}$$

All other equations and the boundary conditions are discretized in the same way. The subscripts i and j denote the X and Y locations, whereas superscripts n and $n+1$ denote the time step. In this study, the numerical computations were carried out for 31×41 grid nodal points with a time step of 10^{-5} and horizontal and vertical step sizes $\Delta X = 1/30$ and $\Delta Y = 1/20$, respectively. The convergence criterion required that the difference between the current and previous iterations for all of the dependent variables be 10^{-4}. In all the results obtained, the enclosure aspect ratio A was taken to be equal to 2.

SOLUTION PROCEDURE

1. All dependent variables are initialized to zero.
2. The new boundary condition values at $n+1$ are calculated for all walls from the previous values at n.
3. The new concentration values at $n+1$ are calculated from the previous n values, and then a subroutine is called to solve the obtained tridiagonal equations for all the concentration values at all the internal grid points.
4. The temperature, vorticity, and the stream function are calculated in the same way as in step 3.
5. The velocity components U and V are calculated at $n+1$ from the values at n explicitly for all the internal grid points.
6. The error is calculated for the concentration, the temperature, and the vorticity at the last time step (only for steady solution).
7. To obtain the solution at the next time step $n+2$, the same procedure is followed starting with step 2. The above procedure is for the unsteady solution. If the steady solution is required, then only the concentration and the temperature are needed to be updated for a number of internal loops for each single time step. Then, at the end of this single time step, the vorticity, the stream function, and the velocity components (U and V) need to be updated.
8. The average Nusselt and Sherwood numbers are then calculated at the left heated wall.

NUMERICAL VALIDATION TESTS

To check the accuracy of the numerical method employed for the solution of the problem under consideration, it was validated (after making the necessary modifications) with the problem of double-diffusive convective flow in a vertical rectangular enclosure with opposing combined temperature and concentration gradients reported earlier by Nishimura et al. [24]. Figures 2*a* and 2*b* present comparisons for the streamlines, isotherms, concentration contours, and density contours of the present work at $N = 0.8$ (thermal-dominated flow) and $N = 1.3$ (compositional-dominated flow) with those reported by Nishimura et al. [24]. Their results for the stream function showed an oscillatory behavior. Table 1 presents a favorable comparison between the present numerical results for a period of oscillation for the stream function extrema at $N = 1$ and those obtained by Morega and Nishimura [25] using the spectral method and by Nishimura et al. [24] using the finite element. These

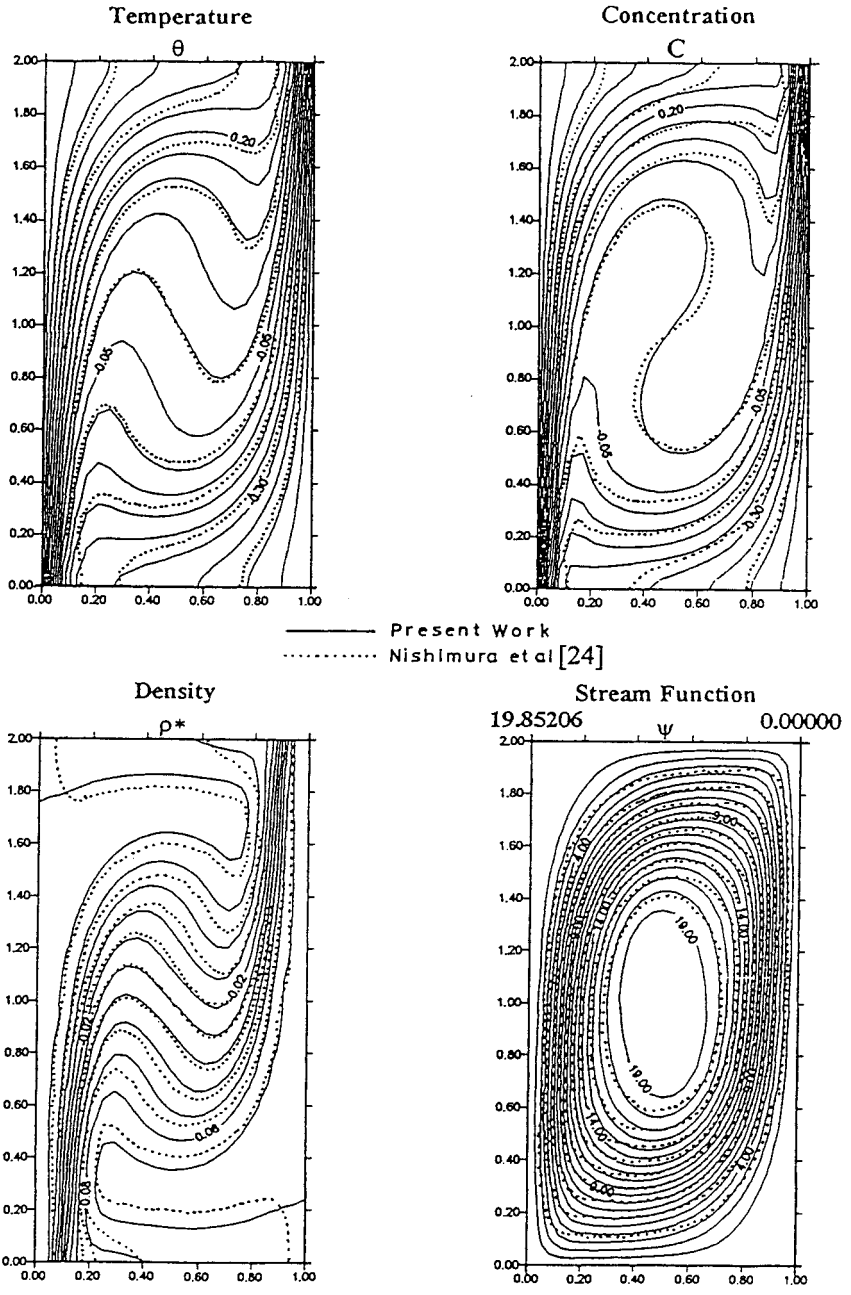

Figure 2*a*. Comparison of thermal-dominated solution with Nishimura et al. [24] for Da*= 0, Le = 2.0, $N = 0.8$, Pr = 1.0, Ra = 10^5, and $\phi = 0$.

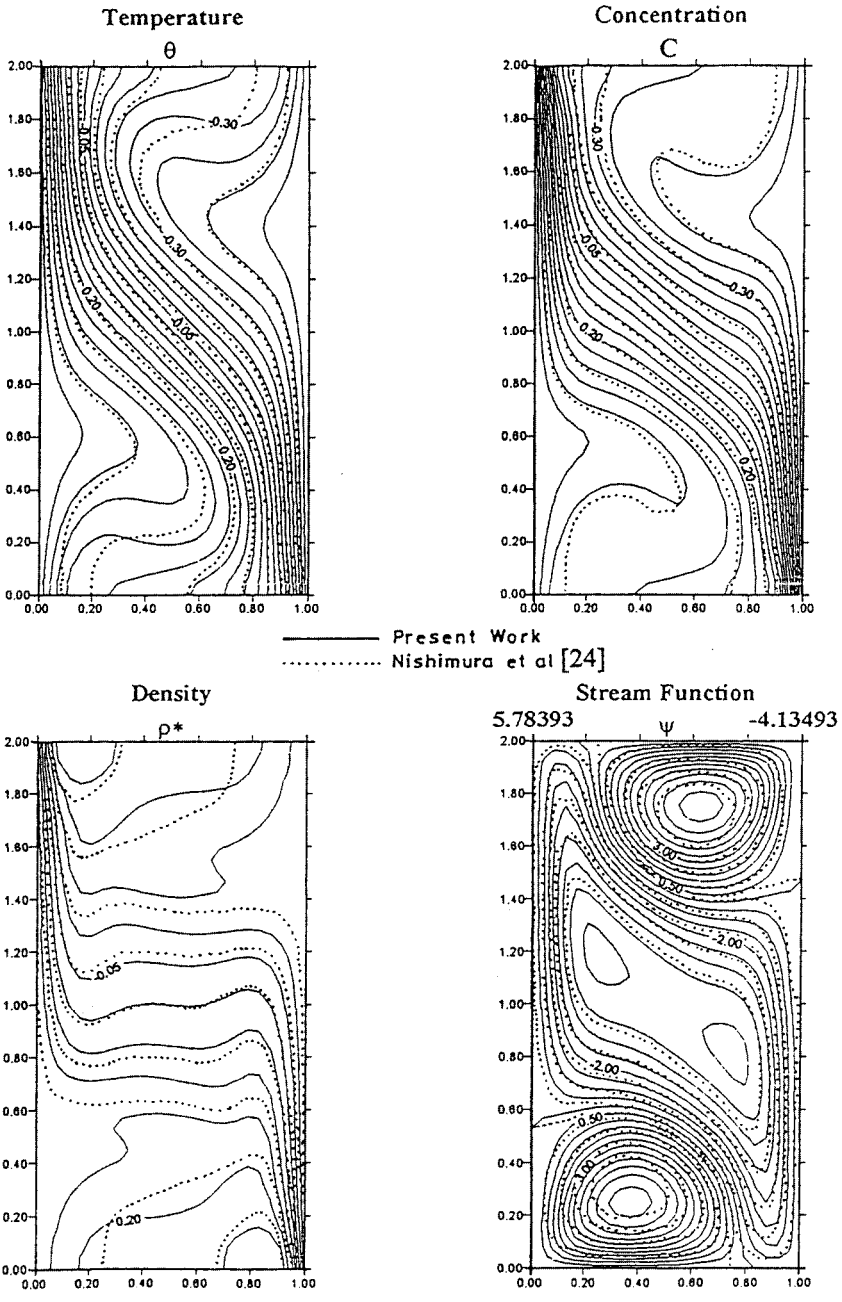

(b)

Figure 2*b*. Comparison of compositional-dominated solution with Nishimura et al. [24] for Da*= 0, Le = 2.0, $N = 1.3$, Pr = 1.0, Ra = 10^5, and $\phi = 0$.

Table 1. Comparison between the present method and two other numerical methods for $N = 1.0$

	Finite element method (31×41 points) Nishimura et al. [24]	Spectral method (40×80 points) Morega and Nishimura [25]	Finite-difference method (31×41 points) current results
τ_0	0.0497	0.0494	0.05091
$\text{Max}\lvert\psi_{max}\rvert$	26.7	26.8	27.2
$\text{Min}\lvert\psi_{max}\rvert$	12.9	12.7	13.7
$\text{Max}\lvert\psi_{min}\rvert$	5.76	5.52	5.85
$\text{Min}\lvert\psi_{min}\rvert$	0.351	0.333	0.333

comparisons show good agreement between the results. This lends confidence into the numerical results to be reported subsequently.

RESULT AND DISCUSSION

In this section, numerical results for the streamline, temperature, and concentration contours as well as selected velocity, temperature, and concentration profiles at midsection of the enclosure for various values of the inverse Darcy number Da*, the dimensionless heat generation or absorption coefficient ϕ, and the buoyancy ratio N will be reported. In addition, representative results for the average Nusselt and Sherwood numbers $\overline{\text{Nu}}$ and $\overline{\text{Sh}}$ at various conditions will be presented in tabulated form and discussed. In all of these results, Le, Pr, and Ra were fixed at the values of 1.0, 0.7, and 10, respectively.

Figure 3 presents steady-state contours for the streamline and temperature for various values of the inverse Darcy number Da* and a buoyancy ratio of unity. Since $\text{Le} = 1$ and $\phi = 0$, the concentration contours are identical to those of temperature and, therefore, are not presented. For the value of the buoyancy ratio N considered the interaction between the thermal and compositional buoyancy effects is significant. In the absence of the porous medium ($\text{Da}^* = 0$), two small recirculations are predicted within the enclosure with both the temperature and concentration contours being horizontally uniform in the core region. However, the presence of the porous medium ($\text{Da}^* \neq 0$) causes the streamline contours to be distorted and the flow to move slower. This is evident from the decreases in the maximum value of the stream function as Da* increases. The distortion effect, which occurs in the clockwise direction, continues causing the formation of a single recirculation in the center of the enclosure as Da* increases. Also, the temperature and concentration contours become more parallel to the vertical walls as Da* increases, indicating the approach to a quasi-conduction regime. It can be concluded that the main contributions of the presence of the porous medium for a buoyancy ratio of unity are predicted to be a flow retardation effect and a suppression of the overall heat transfer in the enclosure.

Representative profiles for the horizontal and vertical components of velocity U and V, temperature θ, and concentration C at the enclosure midsection for various values of Da* for $N = 1.0$ are presented in Figures 4 through 6, respectively. As mentioned before,the presence of the porous medium provides a flow retardation effect. This is manifested by the significant decreases in the net fluid velocity in the

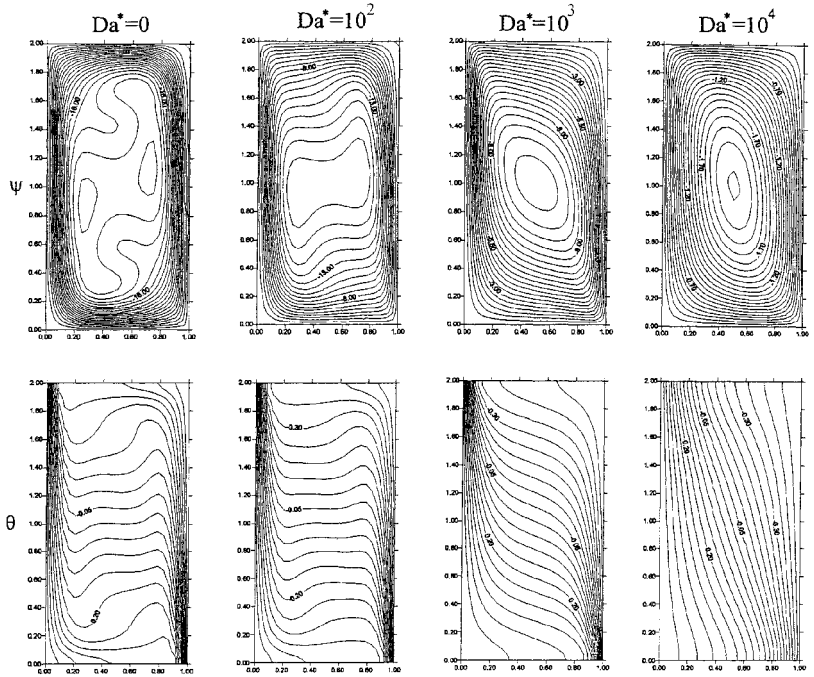

Figure 3. Effects of Da* on the contours of the streamlines, temperature, and concentration for Le = 1.0, $N = 1.0$, Pr = 0.7, Ra = 10^5, and $\phi = 0$.

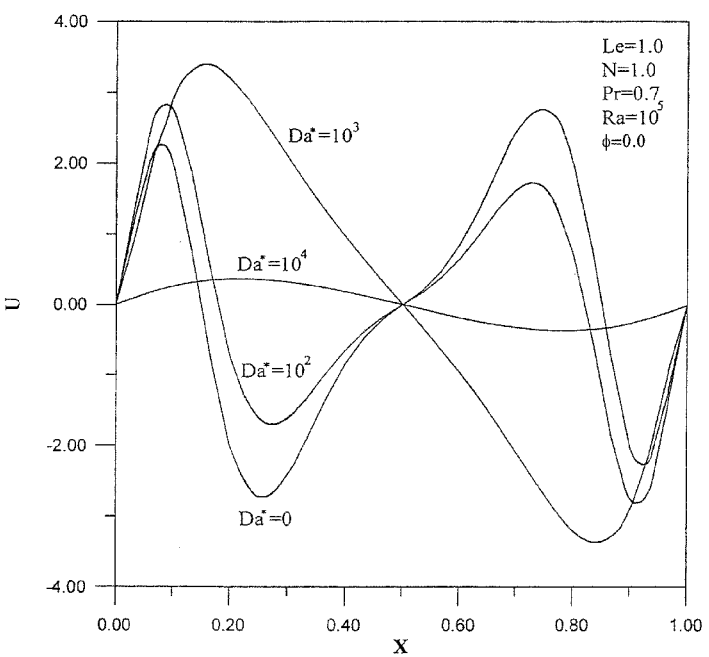

Figure 4. Effects of Da* on horizontal velocity profiles at enclosure midsection.

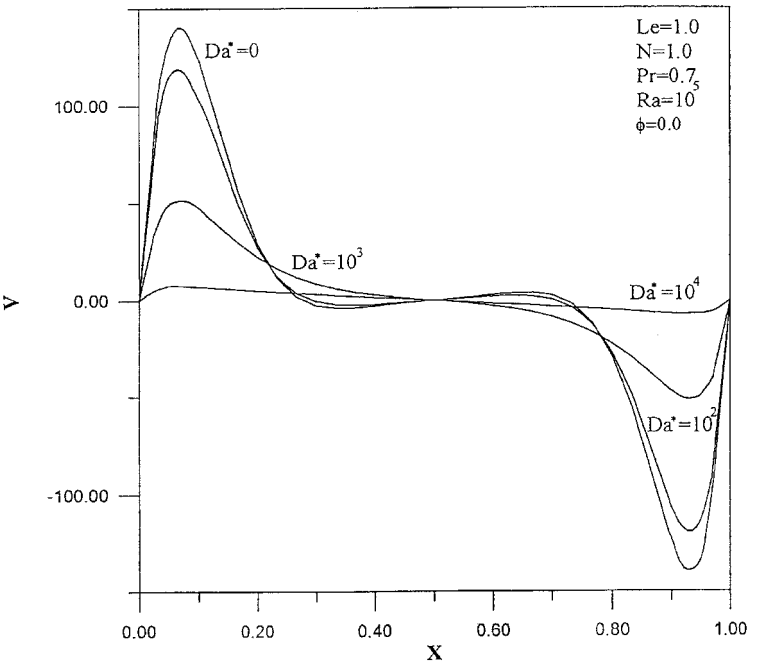

Figure 5. Effects of Da* on vertical velocity profiles at enclosure midsection.

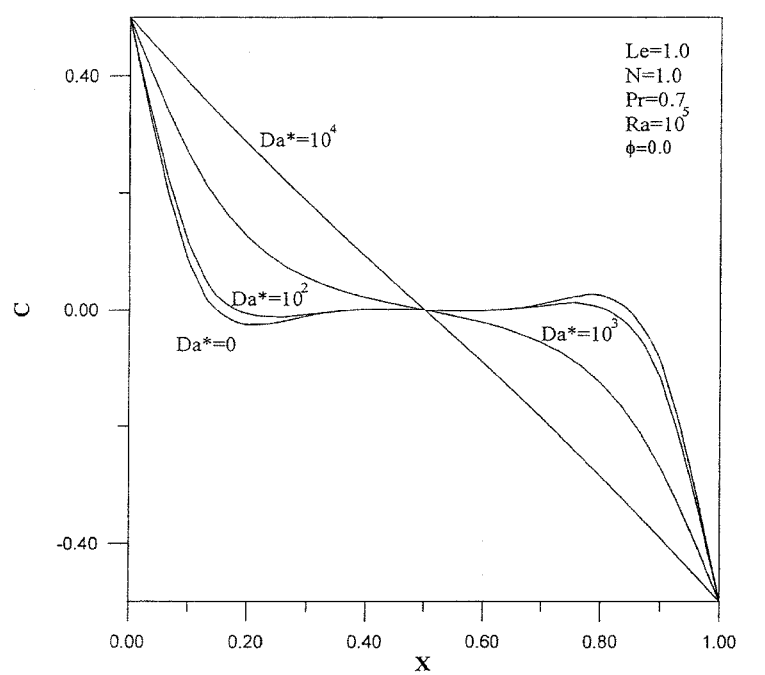

Figure 6. Effects of Da* on temperature or concentration profiles at enclosure midsection.

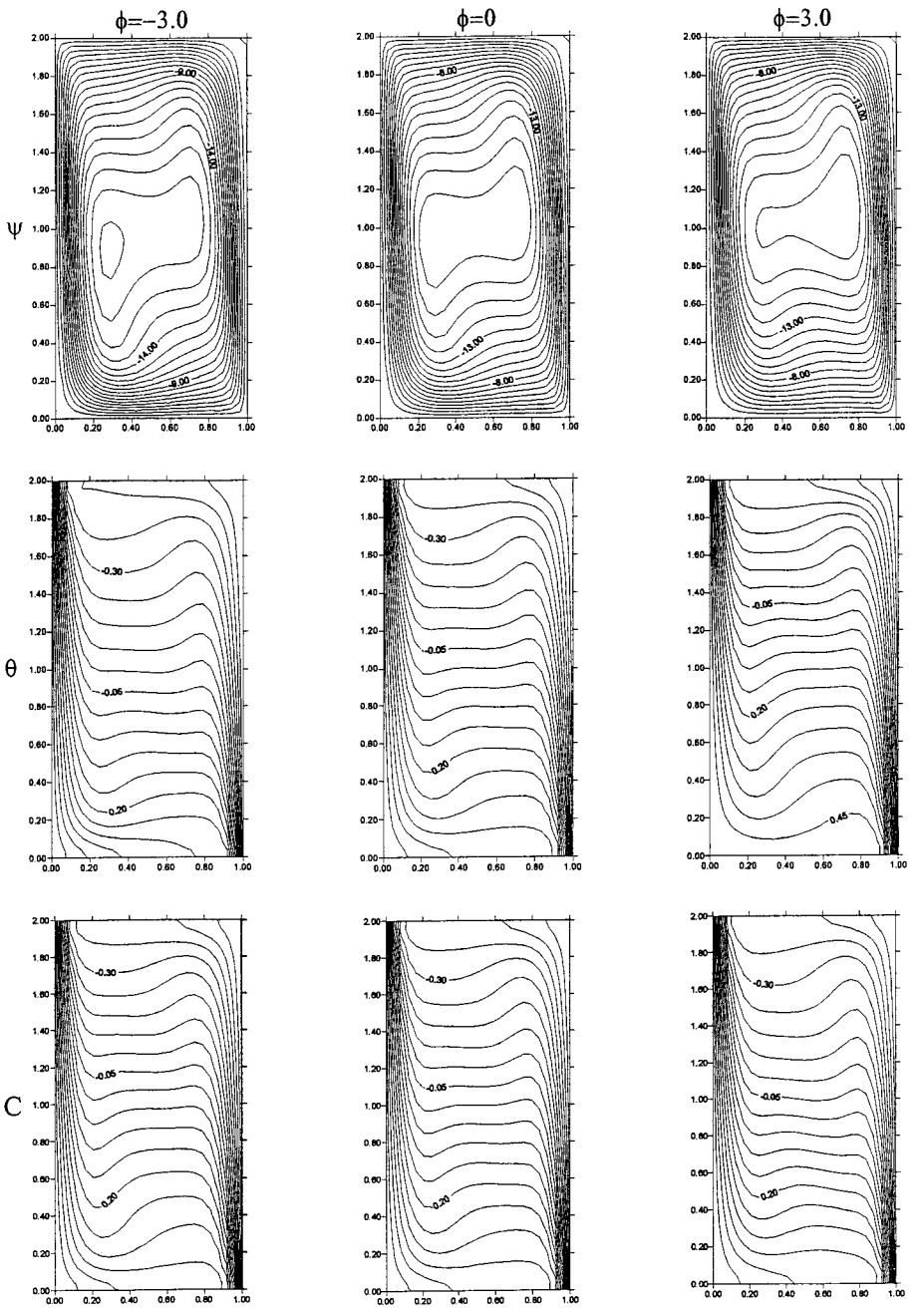

Figure 7. Effects of ϕ on the contours of the streamlines, temperature, and concentration for $Da^* = 10^2$, $Le = 1.0$, $N = 1.0$, $Pr = 0.7$, and $Ra = 10^5$.

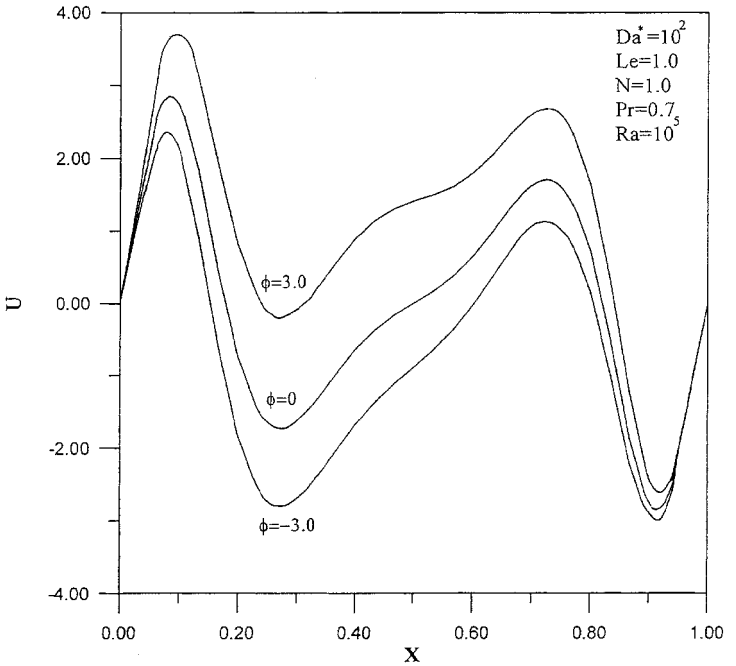

Figure 8. Effects of ϕ on horizontal velocity profiles at enclosure midsection.

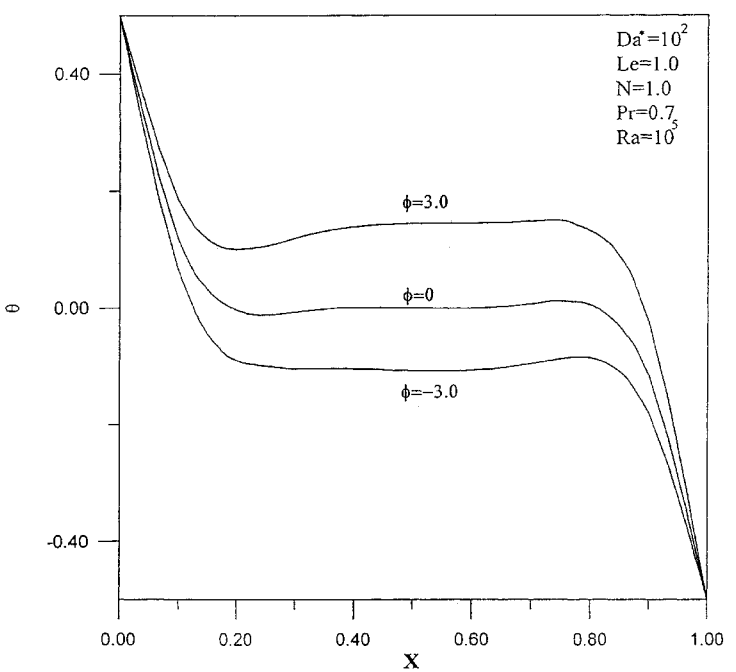

Figure 9. Effects of ϕ on temperature profiles at enclosure midsection.

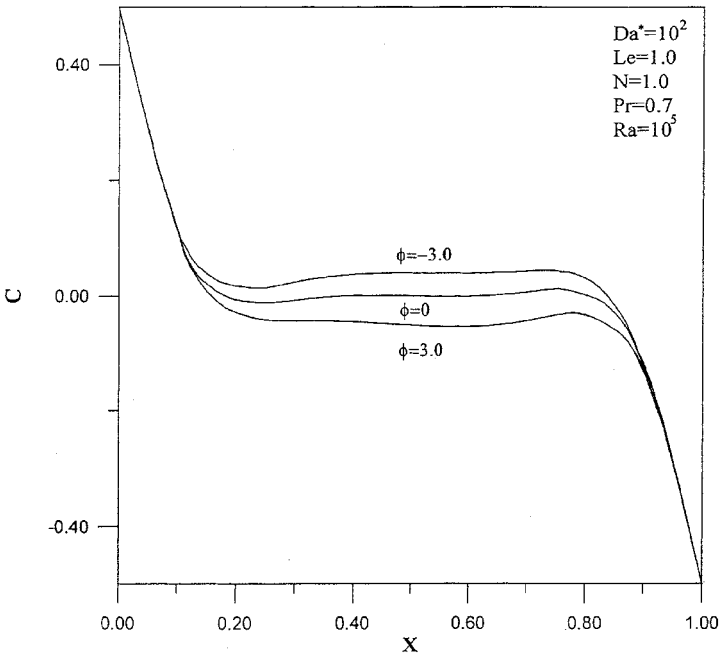

Figure 10. Effects of ϕ on concentration profiles at enclosure midsection.

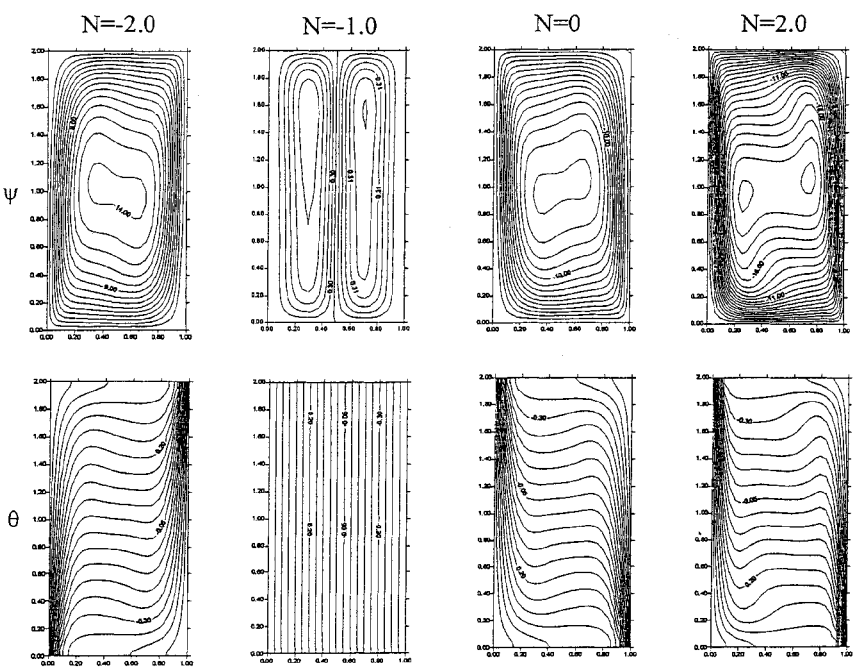

Figure 11. Effects of N on contours of streamlines, temperature, and concentration for $Da^* = 10^2$, Le = 1.0, Pr = 0.7, $Ra = 10^5$, and $\phi = \mathbf{0}$.

vicinity of the heated wall. It can be seen that for $Da^* < 10^3$, the horizontal velocity component increases while the normal velocity component decreases as Da* increases. However, for $Da^* > 10^3$ both the horizontal and normal velocity components decrease as Da* increases. In both ranges, the net velocity decreases as Da* increases. For $\phi = 0$ and $Le = 1$, the equations governing the temperature and concentration and their boundary conditions become the same. Therefore, their profiles at the enclosure midsection become the same. It is seen that the presence of the porous medium causes both the temperature and concentration to increase until their profiles become linear, which indicates the limit of "no flow." These behaviors are illustrated in Figure 6.

Figure 7 displays the contours for the streamline, temperature, and concentration for three different values of the dimensionless heat generation or absorption coefficient ϕ, respectively. For $\phi = 0$, the streamlines are characterized by a single recirculating vortex in the middle of the enclosure stretched symmetrically in the horizontal direction. For $\phi = 3$ (heat generation), the vortex tends to move toward the right wall, while for $\phi = -3$ (heat absorption), it moves toward the left heated wall. An inspection of the maximum value of the stream function for $\phi = -3$, 0, and 3 reveals that it is highest for $\phi = -3$ and decreases as ϕ increases. This indicates that the flow is fastest for $\phi = -3$ and starts to slow down as ϕ increases. The contours for temperature and concentration show that increasing the value of ϕ has a greater effect on temperature than concentration and that the isotherms become less horizontally uniform in the lower portion of the cavity.

Figures 8 through 10 display the effects of the dimensionless heat generation or absorption coefficient ϕ on the horizontal velocity, temperature, and concentration, respectively. The presence of a heat source within the enclosure causes the fluid temperature to increase significantly and the concentration to decrease slightly everywhere in the enclosure except at the walls, which are fixed by the boundary conditions as shown in Figures 9 and 10. The increase in the temperature causes the thermal buoyancy effect to increase while the decrease in the concentration produces lower compositional buoyancy effect. At $N = 1$, the thermal buoyancy effect is higher than that of the compositional effect. This net increase in the buoyancy effect due to the presence of a heat source (heat generation) in the enclosure induces more flow there. This is depicted by the increases in the horizontal velocity shown in Figure 8 as ϕ increases. The presence of a heat sink within the enclosure produces the exact opposite effect.

Figure 11 illustrates the effects of the buoyancy ratio N on the contours of the streamlines and temperature (or concentration) for $Da^* = 100$ and $\phi = 0$. The streamlines show a transitional behavior from a single vortex in the whole enclosure for $N = -2.0$ (opposing flow) and $N = 0$ (thermal-buoyancy flow) to two separate vortices for $N = -1.0$ and two nonseparated vortices for $N = 2.0$ (aiding flow). The maximum intensity of the flow is predicted to decrease as N increases. The isotherms and the isoconcentration lines (which are the same as explained before) show that significant changes occur in the boundary-layer regions close to the walls and that in the enclosure core region the isotherms and isoconcentration lines are parallel to the horizontal walls for $N \neq -1.0$. However, for $N = -1.0$, these lines are all parallel to the enclosure vertical walls. This indicates that for this value of N, the flow is induced only by conduction.

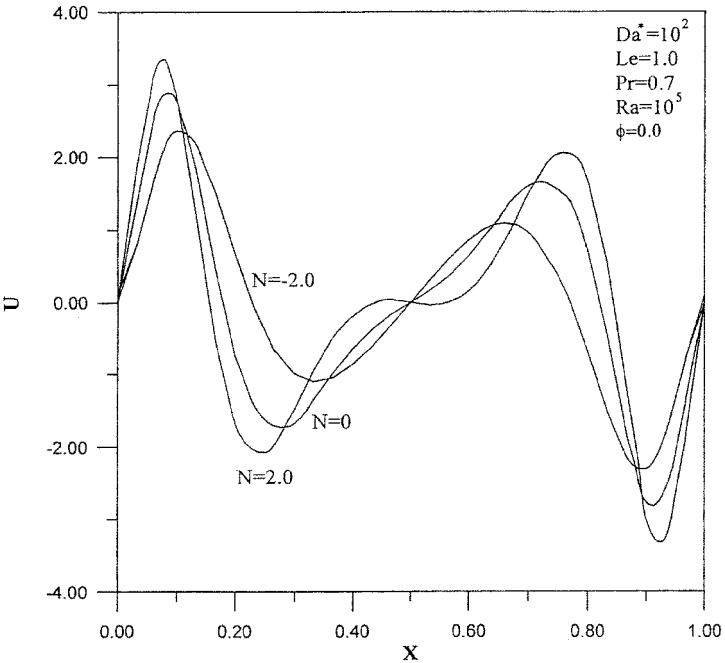

Figure 12. Effects of N on horizontal velocity profiles at enclosure midsection.

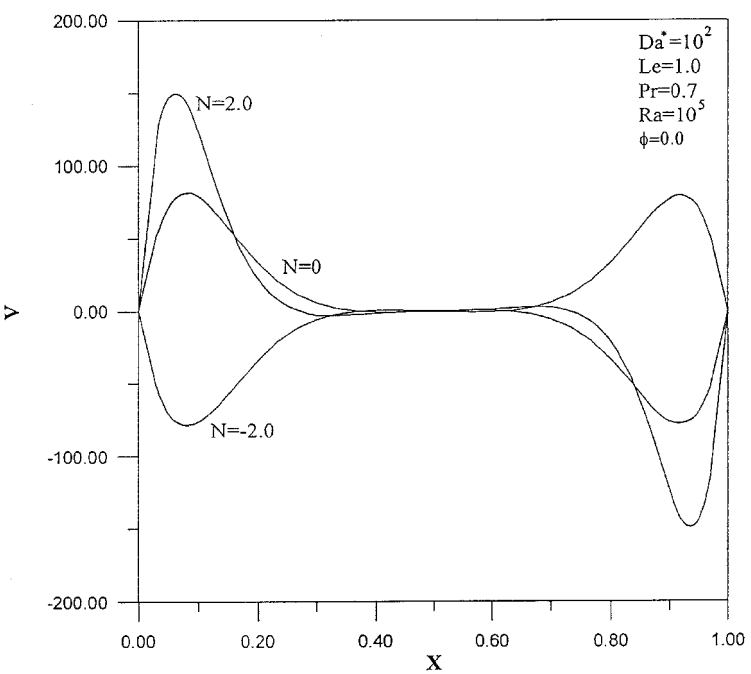

Figure 13. Effects of N on vertical velocity profiles at enclosure midsection.

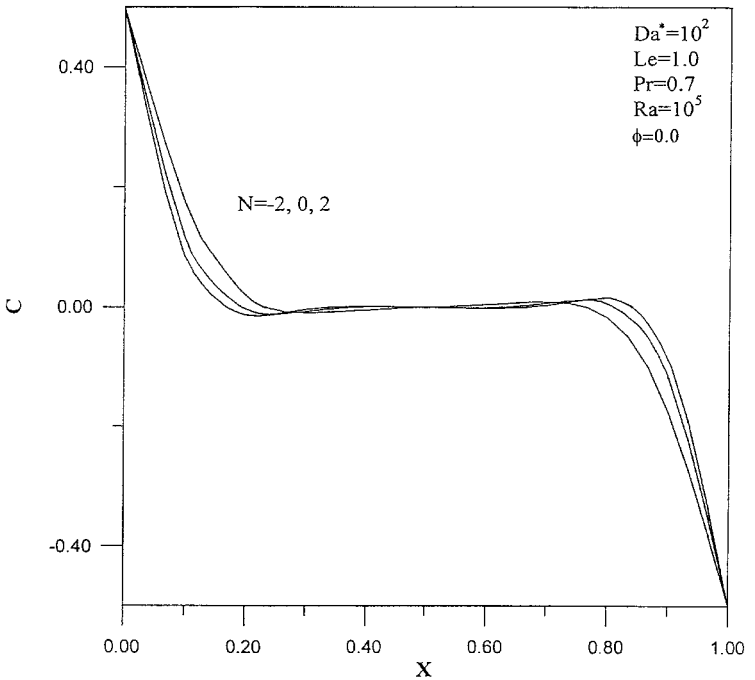

Figure 14. Effects of N on temperature or concentration profiles at enclosure midsection.

Figures 12 through 14 depict the influence of N on the horizontal velocity U, vertical velocity V, and temperature θ (or concentration C) profiles, respectively. It can be observed that the peak values of U and V near the hot wall tend to increase as N increases. However, the temperature (or concentration) profiles show that they decrease there as N increases.

The effects of the inverse Darcy number Da* and the dimensionless heat generation or absorption coefficient ϕ on the average Nusselt number $\overline{\mathrm{Nu}}$ and the average Sherwood number $\overline{\mathrm{Sh}}$ for a buoyancy ratio $N = 1.0$ are presented in Tables 2 and 3, respectively. It is observed that both $\overline{\mathrm{Nu}}$ and $\overline{\mathrm{Sh}}$ have a decreasing trend with increases in Da*. The values of $\overline{\mathrm{Nu}}$ and $\overline{\mathrm{Sh}}$ are identical because for $\phi = 0$ and Le = 1, the equations governing the temperature and concentration are exactly

Table 2. Effects of Da* on the average Nusselt and Sherwood numbers at the heated wall of the cavity for Le = 1.0, N = 1.0, Pr = 0.7, Ra = 10^5, and ϕ = **0**

Parameter	$\overline{\mathrm{Nu}}$	$\overline{\mathrm{Sh}}$
Da* = 0	6.08899	6.08899
Da* = 10^2	5.59823	5.59823
Da* = 10^3	3.59821	3.59821
Da* = 10^4	1.26309	1.26309

similar. These behaviors are clearly shown in Table 2. In addition, the presence of a heat source within the enclosure has the tendency to decrease the negative temperature and concentration gradients at the hot wall, resulting in reductions in both $\overline{Nu}$ and $\overline{Sh}$. On the other hand, the presence of a heat sink within the enclosure produces the opposite effect, namely, it increases in both $\overline{Nu}$ and $\overline{Sh}$. This is true for all values of Da* as seen from Tables 3*a* through 3*d*. As mentioned before, the effect of ϕ on the temperature distribution is much greater than that on the concentration distribution. This is reflected by the large changes in $\overline{Nu}$ and the small changes in $\overline{Sh}$ as ϕ is altered.

Table 3*a*. Effects of ϕ on the average Nusselt and Sherwood numbers at the heated wall of the cavity for Da* = 0, Le = 1.0, N = 1.0, Pr = 0.7, and Ra = 10^5

Parameter	$\overline{Nu}$	$\overline{Sh}$
$\phi = -3.0$	6.73202	6.11236
$\phi = 0.0$	6.08899	6.08899
$\phi = 3.0$	5.21513	6.03596

Table 3*b*. Effects of ϕ on the average Nusselt and Sherwood numbers at the heated wall of the cavity for Da* = 10^2, Le = 1.0, N = 1.0, Pr = 0.7, and Ra = 10^5

Parameter	$\overline{Nu}$	$\overline{Sh}$
$\phi = -3.0$	6.21445	5.61958
$\phi = 0.0$	5.59823	5.59823
$\phi = 3.0$	4.80802	5.53928

Table 3*c*. Effects of ϕ on the average Nusselt and Sherwood numbers at the heated wall of the cavity for Da* = 10^3, Le = 1.0, N = 1.0, Pr = 0.7, and Ra = 10^5

Parameter	$\overline{Nu}$	$\overline{Sh}$
$\phi = -3.0$	4.18530	3.60811
$\phi = 0.0$	3.59821	3.59821
$\phi = 3.0$	2.83844	3.56185

Table 3*d*. Effects of ϕ on the average Nusselt and Sherwood numbers at the heated wall of the cavity for Da* = 10^4, Le = 1.0, N = 1.0, Pr = 0.7, and Ra = 10^5

Parameter	$\overline{Nu}$	$\overline{Sh}$
$\phi = -3.0$	2.03523	1.25663
$\phi = 0.0$	1.26309	1.26309
$\phi = 3.0$	0.15255	1.26811

Table 4. Effects of N on the average Nusselt and Sherwood numbers at the heated wall of the cavity for Da* = 100, Le = 1.0, Pr = 0.7, Ra = 10^5, and $\phi = 0$

Parameter	$\overline{\mathrm{Nu}}$	$\overline{\mathrm{Sh}}$
N = −2.0	4.37746	4.37746
N = −1.0	0.99975	0.99975
N = 0.0	4.37789	4.37789
N = 1.0	5.59823	5.59823
N = 2.0	6.48282	6.48282

Table 4 depicts the influence of the buoyancy ratio N on the values of $\overline{\mathrm{Nu}}$ and $\overline{\mathrm{Sh}}$ for Da* = 100, Le = 1.0, and $\phi = 0$. As mentioned before, for these values and regardless of the value of Da*, the values of $\overline{\mathrm{Nu}}$ and $\overline{\mathrm{Sh}}$ are the same. It is predicted that increases in the buoyancy ratio N produce higher values of $\overline{\mathrm{Nu}}$ and $\overline{\mathrm{Sh}}$ for aiding flow situations ($N > 0$). However, for opposing flow situations ($N < 0$), it is predicted that $\overline{\mathrm{Nu}}$ and $\overline{\mathrm{Sh}}$ are minimum for $N = -1.0$ and that they increase for values of N greater or less than this critical value.

CONCLUSIONS

The problem of double-diffusive convective flow of a binary gas-particle mixture inside a rectangular porous enclosure with cooperating temperature and concentration gradients and in the presence of heat generation or absorption effects was studied numerically using the finite-difference method. Comparisons with previously published work on modified cases of the problem were performed and found to be in good agreement. Graphic results for the streamline, temperature, and concentration contours and representative velocity, temperature, and concentration profiles at the enclosure midsection for various parametric conditions were presented and discussed. It was found that the heat and mass transfer and the flow characteristics inside the enclosure depended strongly on the inverse Darcy number and the heat generation or absorption effects. The presence of the porous medium was found to reduce the average Nusselt and Sherwood numbers and the fluid circulation within the enclosure. In addition, it was concluded that the average Nusselt and Sherwood numbers decreased as a result of heat generation and increased as a result of heat absorption. Furthermore, the presence of heat generation or absorption effects had greater influence on the average Nusselt number than on the average Sherwood number. Increasing the buoyancy ratio was predicted to increase both the average Nusselt and Sherwood numbers for aiding flow situations while minimum values are predicted for opposing flow situations.

REFERENCES

1. C. Beghein, F. Haghighat, and F. Allard, Numerical Study of Double-Diffusive Natural Convection in a Square Cavity, *Int. J. Heat Mass Transfer*, vol. 35, pp. 833–846, 1992.
2. S. Ostrach, Natural Convection with Combined Driving Forces, *PhysicoChem. Hydrodyn.*, vol. 1, pp. 233–247, 1980.

3. R. Viskanta, T. L. Bergman, and F. P. Incropera, Double-Diffusive Natural Convection, in (eds.), S. Kakac, W. Aung, and R. Viskanta, *Natural Convection: Fundamentals and Applications*, pp. 1075–1099, Hemisphere, Washington, DC, 1985.
4. J. W. Lee and J. M. Hyun, Double-Diffusive Convection in a Rectangle with Opposing Horizontal and Concentration Gradients, *Int. J. Heat Mass Transfer*, vol. 33, pp. 1619–1632, 1990.
5. J. M. Hyun and J. W. Lee, Double-Diffusive Convection in a Rectangle with Cooperating Horizontal Gradients of Temperature and Concentration Gradients, *Int. J. Heat Mass Transfer*, vol. 33, pp. 1605–1617, 1990.
6. M. Mamou, P. Vasseur, and E. Bilgen, Analytical and Numerical Study of Double Diffusive Convection in a Vertical Enclosure, *Heat and Mass Transfer*, vol. 32, pp. 115–125, 1996.
7. C. W. Lan and C. Y. Tu, Morphological Instability due to Double Diffusive Convection in Directional Solidification: The Pit Formation, *J. Crystal Growth*, vol. 220, pp. 619–630, 2000.
8. S. Mergui and D. Gobin, Transient Double Diffusive Convection in a Vertical Enclosure with Asymmetrical Boundary Conditions, *J. Heat Transfer*, vol. 122, pp. 598–602, 2000.
9. I. Sezai and A. A. Mohamad, Double Diffusive Convection in a Cubic Enclosure with Opposing Temperature and Concentration Gradients, *Physics of Fluids*, vol. 12, pp. 2210–2223, 2000.
10. L. W. Wang, C. Y. Wei, J. H. Lin, and S. L. Wang, Double-Diffusive Convection in an Annular Enclosure with a Hot Inner Cylinder, *Experimental Heat Transfer*, vol. 11, pp. 329–340, 1998.
11. M. Mamou, P. Vasseur, and E. Bilgen, A Galerkin Finite-Element Study of the Onset of Double-Diffusive Convection in an Inclined Porous Enclosure, *Int. J. Heat Mass Transfer*, vol. 41, pp. 1513–1529, 1998.
12. O. V. Trevisan and A. Bejan, Mass and Heat Transfer by Natural Convection in a Vertical Slot Filled with Porous Medium, *Int. J. Heat Mass Transfer*, vol. 29, pp. 403–415, 1986.
13. F. Chen and C. Chen, Double-Diffusive Fingering Convection in a Porous Medium, *Journal of Heat Transfer*, vol. 36, pp. 793–897, 1993.
14. D. Lin, Unsteady Natural Convection Heat and Mass Transfer in a Saturated Porous Enclosure, *Warme-und-stoffubertragung*, vol. 28, pp. 49–56, 1993.
15. M. Mamou, P. Vasseur, E. Bilgen, and D. Gobin, Double Diffusive Convection in an Inclined Slot Filled with Porous Medium, *European Journal of Mechanics/Fluids*, vol. 14, pp. 629–652, 1995.
16. M. Marcoux, M.-C. Charrier-Mojtabi, and M. Azaiez, Double Diffusive Convection in an Annular Vertical Porous Layer, *Int. J. Heat Mass Transfer*, vol. 42, pp. 2313–2325, 1999.
17. I. S. Shivakumara and R. Sumithra, Non-Darcian Effects on Double Diffusive Convection in a Sparsely Packed Porous Medium, *Acta Mechanica*, vol. 132, pp. 113–127, 1999.
18. A. Mahidjiba, M. Mamou, and P. Vasseur, Onset of Double-Diffusive Convection in a Rectangular Porous Cavity Subject to Mixed Boundary Conditions, *Int. J. Heat Mass Transfer*, vol. 43, pp. 1505–1522, 2000.
19. S. Kakac, W. Aung, and R. Viskanta, *Natural Convection-Fundamentals and Applications*, Hemisphere, Washington, DC, 1985.
20. S. Acharya and R. J. Goldstein, Natural Convection in an Externally Heated Vertical or Inclined Square Box Containing Internal Energy Sources, *ASME J. Heat Transfer*, vol. 107, pp. 855–866, 1985.

21. A. G. Churbanov, P. N. Vabishchevich, V. V. Chudanov, and V. F. Strizhov, A Numerical Study on Natural Convection of a Heat-Generating Fluid in Rectangular Enclosures, *Int. J. Heat Mass Transfer*, vol. 37, pp. 2969–2984, 1994.
22. K. Vajravelu and J. Nayfeh, Hydromagnetic Convection at a Cone and a Wedge, *Int. Commun. Heat Mass Transfer*, vol. 19, pp. 701–710, 1992.
23. A. J. Chamkha, Non-Darcy Fully Developed Mixed Convection in a Porous Medium Channel with Heat Generation/Absorption and Hydromagnetic Effects, *Numer. Heat Transfer*, vol. 32, pp. 653–675, 1997.
24. T. Nishimura, M. Wakamatsu, and A. M. Morega, Oscillatory Double-Diffusive Convection in a Rectangular Enclosure with Combined Horizontal Temperature and Concentration Gradients, *Int. J. Heat Mass Transfer*, vol. 4l, pp. 1601–1611, 1998.
25. A. M. Morega and T. Nishimura, Double-Diffusive Convection by Chebyshev Collocation Method, *Technology Reports of the Yamaguchi University*, vol. 5, pp. 259–276, 1996.